<Friction Stir Welding and Processing> <K.V. Jata, M. Mahoney, R. Mishra>
TMS (The Minerals, Metals & Materials Society, <2003>

Thermo-Mechanical Processing in Friction Stir Welds

J.A. Schneider[1], A.C. Nunes, Jr., [2]

[1] Mechanical Engineering Department
Mississippi State University
Mississippi State, MS 39762
[2] Materials, Processes and Manufacturing
Metallic Materials
NASA-Marshall Space Flight Center
Huntsville, AL 35812

Abstract

In Friction Stir Welding (FSW) a rotating pin-tool inserted into a weld seam literally stirs the edges of the seam together. In this study, two flow paths are proposed that define the FWS zone. Studies using a longitudinal tungsten wire (0.0025" dia.) were used to visualize and document the material flow. The material flow path is described using a mathematical model.

Introduction

Friction stir welding is a solid-phase joining, or welding process that was invented in 1991 at The Welding Institute (TWI) [1]. The process is potentially capable of joining a wide variety of aluminum alloys that are traditionally difficult to fusion weld. The friction stir welding (FSW) process produces welds by moving a non-consumable rotating pin tool along a seam between work pieces that are firmly clamped to an anvil. At the start of the process, the rotating pin is plunged into the material to a pre-determined load. The mechanical work of the pin transformed to heat raises the temperature thereby softening the weld metal adjacent to the tool. The load on the tool shoulder and the supporting anvil reaction maintain a high hydrostatic pressure as the metal is literally stirred together. To produce a defect free weld, process variables (RPM, travel speed, and downward force) and tool pin design must be chosen carefully. An accurate model of the material flow during the process is necessary to guide process variable selection.

Observations of weld macrostructural features and the results of tracer experiments have provided a basis for the construction of a plastic slip line model of the friction stir welding process at Marshall Space Flight Center [2]. Although the model appears to have

captured the main macrostructural features of the process, the microstructural features and the underlying material specific interactions are not yet understood.

The macroscopic features of the cross-section of a friction stir weld are typically described as an outer heat affected zone (HAZ), an inner thermo-mechanically affected zone (TMAZ), and a central nugget of fine, equiaxed grains. A striking feature of the FSW microstructure is a central nugget, shown in Figure 1. Under a light microscope, this central nugget displays contrasting layers of varying thickness, like onion rings. The shape and spacing of the layers are reported [3] to vary with the ratio of weld velocity (V) to pin rotational speed (Ω) . The same layers can also be observed in a lateral section of the weld shown in Figure 2, where they are reported to have a spacing equal to the increment of pin travel per tool rotation.

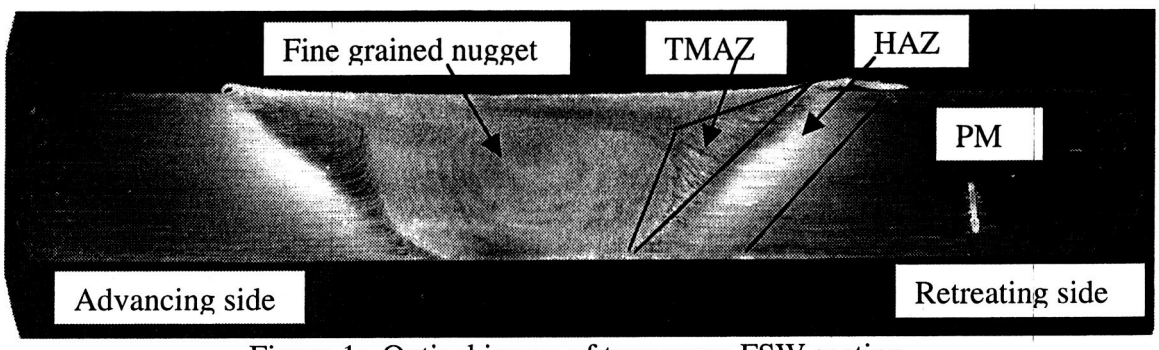

Figure 1: Optical image of transverse FSW section.

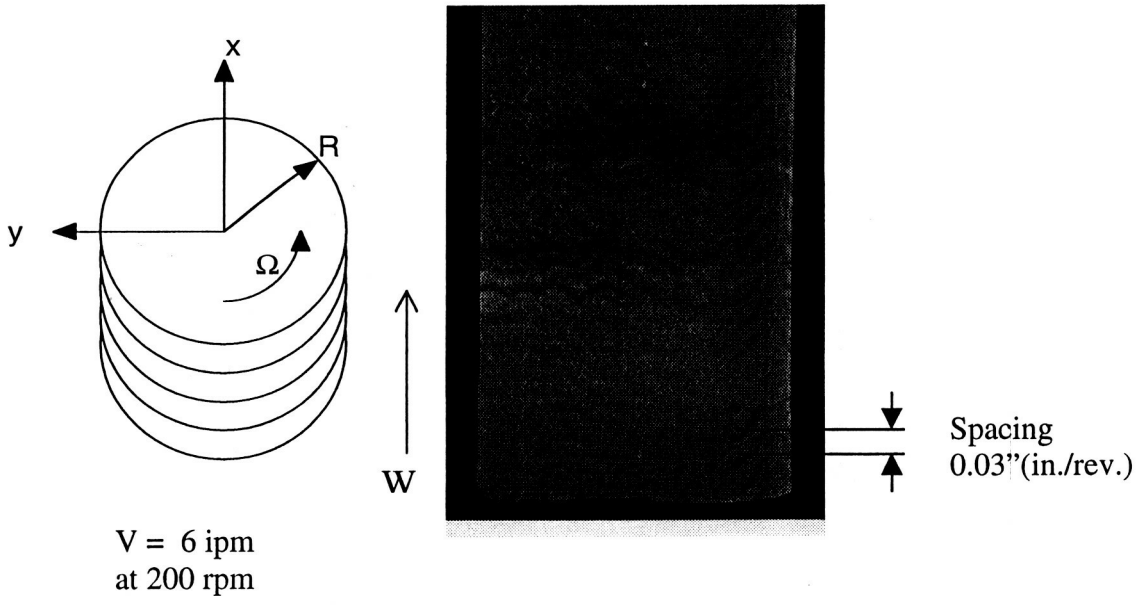

Figure 2: Optical image of lateral section of the FSW.

Microscopically the grain morphology shows a transition in the transverse section from the 80 to 100 μm elongated grains of the parent material (PM) to 0.5-10 μm equiaxed grains within the nugget. Figure 3 shows this transition between the TMAZ and nugget to be quite sharp in transverse section. The deformation of the base metal in the TMAZ manifests itself merely as bending of the grains.

Several FSW flow visualization studies have been reported in the literature using either dissimilar materials or tracer techniques. Li et al., [4, 5] describe patterns observed on FSW transverse sections made between dissimilar Al alloys and between Al alloys and Cu. Differential etching of the dissimilar materials reveal material flow patterns, described as a "chaotic-dynamic mixing".

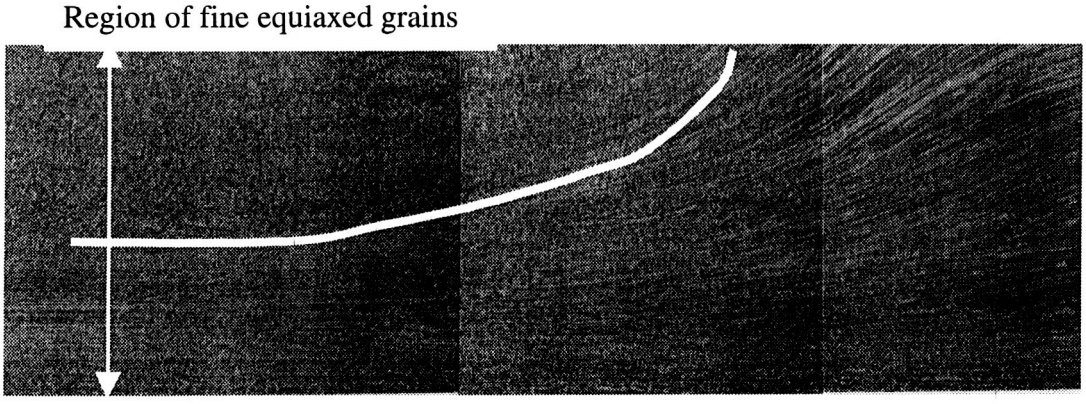

Figure 3: Optical image of sharp demarcation from elongated grains into the fine grained, retreating side of the nugget.

Colligan [6] studied the material flow using steel shot embedded prior to welding in a groove parallel to the weld direction and intersecting various positions on the transverse section. This approach allowed FSW flow trajectories to be followed by post weld x-ray inspection. Colligan inferred that material from the upper portion of the weld is stirred and forced downward by the pin threads, but that much of the weld metal is simply extruded around the pin. The 0.015" dia. steel shot limits the resolution of this study. The shot cannot follow flows closer to the pin than the order of 0.015" or very high flow gradients.

Seidel and Reynolds [7] utilized a marker insertion technique to investigate the flow around the pin tool. The after-FSW, three-dimensional marker configuration was reconstructed from a series of section images.

Flow visualization studies all indicate the flow field around a FSW tool is complicated. But there is too much order in the marker patterns subjected to FSW for a random shuffling of metal. The weld metal appears to flow along defined paths or streamlines.

A model [2] that seems to represent the essential macroscopic features of the flow field around the FSW pin-tool may be synthesized from three incompressible flow fields that combine to fit the boundary conditions about the FSW pin-tool.

The first of the three fields comprises a rigid-body rotation identical to the rotation of the tool spindle and bounded by a cylindrical shear surface, a velocity discontinuity between the rotating plug of metal attached to the tool and the motionless surroundings. The shear surface discontinuity is essentially the one slip line in a classical plastic slip line FSW model. The shear surface is the analogue of the "line of shear" between the metal to be cut and the chip in an elementary model of the machining process. (A FSW analogue of a metal-cutting chip is a stream tube of metal, i.e. a region bounded by two streamlines, inside the rotating plug of metal next to the tool.)

The second of the three fields is a homogeneous and isotropic velocity field with the velocity equal and opposite to the travel velocity of the weld-tool. The superposition of the first and second velocity fields yields a flow field in which an element of weld metal progresses slowly up to the pin in a straight line, rapidly rotates around the retreating side of the pin in a circular arc, and slowly recedes from the rear of the pin in a straight line, a continuation of the line of approach.

The third of the three fields is a ring vortex flow, or Maelstrom flow about the tool. It is clear from marker studies that metal moves up and down in the vicinity of the tool. The first two flow fields are planar with no up-and-own components. It is the third flow field, the ring vortex, that induces the up-and–down motion. Driven by the typical thread configuration the streamlines flow down at the tool, out at the tool bottom, up outside the tool, and back in at the top of the tool under the tool shoulder for closure. Equivalent streamlines mark out a donut or smoke-ring shape, the ring vortex, around the pin. Superposed upon the other two flow fields the ring vortex field can induce very complex motions. For example, the inward velocity component of the ring vortex can prevent metal from exiting the rotating plug, forcing it to spiral down the tool with a different thermo-mechanical history and a different microstructure from metal that passes by in a fraction of a rotation on the retreating side of the pin. This downward spiraling current is called the "maelstrom' to distinguish it from the "straight-through" current. The hypothetical flow field components and resultant (tracer-observable) flow currents are shown schematically in Figure 4 .

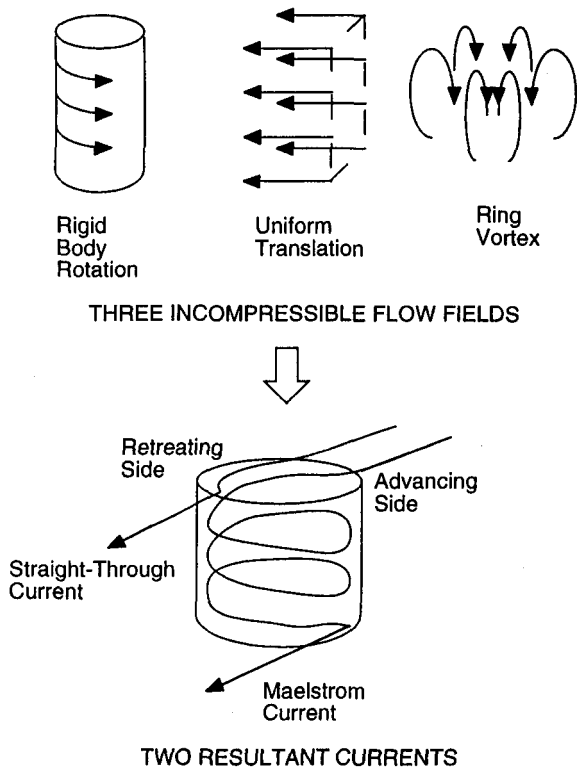

Figure 4. Hypothetical flow fields and resultant currents in the neighborhood of the friction stir welding tool.

The above three-field model explains the general, macroscopic features of the marker experiments cited above, but more detail is needed if the microscopic features of the flow are to be dealt with. In considering how to obtain more detailed information on the flow in the vicinity of the FSW pin-tool the authors hit upon a technique that appears to have some promise for investigating this flow.

Instead of the shot markers embedded by Kevin Colligan in the faying surface of a FSW seam a thin (0.0025 inch diameter) tungsten wire was inserted. The wire offers the advantages of being more convenient to manipulate than the shot. It can be pressed in place without the necessity of cutting a groove, and it is appreciably finer than the 0.015 inch diameter shot used by Colligan for better resolution. Smaller particles might replace the shot, but presumably at a cost in difficulty in manipulation.

If the shear zone stresses are severe enough, the wire will break. A stiff wire breaks in bending; a flexible wire, in tension as shown in Fig. 5. The size of the resulting segments can be estimated based on the assumptions that it exhibits either brittle or ductile behavior.

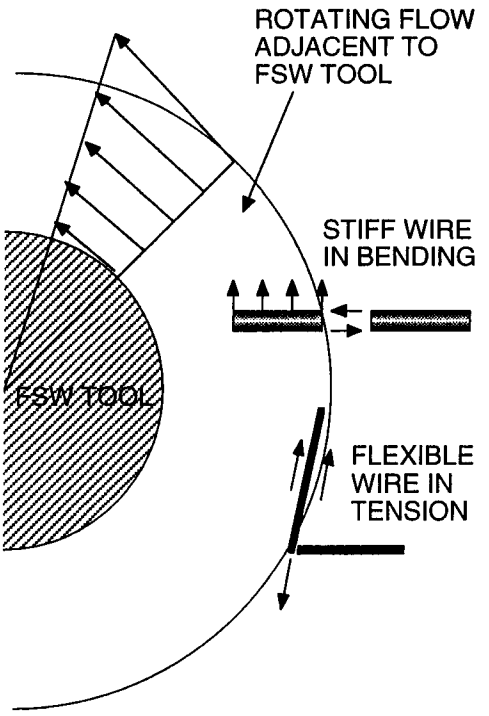

Figure 5. Fracture loading configurations for a stiff wire and a flexible wire encountering the flow field adjacent to the FSW tool.

Suppose that the wire is stiff and extends out into a transverse flow of moving weld metal. The maximum tensile stress, σ_{wire}, in the wire treated like a cantilever beam with a load per unit area equal to the double the pressure, approximately $3\sigma_{weld}$, of the weld metal to indent the surface, depends upon the length of the beam ΔL. In equation 1 the moment imposed on the wire by the weld metal flowing around it is equated to the moment generated at the wire cross section to balance it.

$$\int_0^{\Delta L} \underbrace{6\sigma_{weld}}_{\text{estimated pressure}} \underbrace{(2rdx)}_{\text{area increment}} \underbrace{x}_{\text{moment arm}} \sim \int_{-\frac{\pi}{2}}^{+\frac{\pi}{2}} \underbrace{\sigma_{wire}\sin\theta}_{\text{local stress}} \underbrace{[2r\cos\theta d(r\sin\theta)]}_{\text{area increment}} \underbrace{r\sin\theta}_{\text{moment arm}} \qquad \textbf{(1a)}$$

$$6\sigma_{weld} r(\Delta L)^2 \sim \frac{\pi\sigma_{wire} r^3}{4} \qquad \textbf{(1b)}$$

$$\Delta L \sim r\sqrt{\frac{\pi}{24}\frac{\sigma_{wire}}{\sigma_{weld}}} \qquad \textbf{(1c)}$$

If σ_{wire} is taken as the fracture stress of the wire, ΔL is the length at which the wire fractures and the length of the broken wire segments trailing the pin-tool.

Suppose that the wire is very flexible, supports no moment, and extends parallel to the flow velocity. If the weld metal adheres to its surface, the shear stress of the flowing metal exerted on the wire surface is approximately $\frac{\sigma_{weld}}{2}$. As the wire segment immersed in the flowing metal lengthens the force on the wire, which must be supported by the wire cross-section, grows until the wire fractures. In equation 2 the force imposed on the wire by the weld metal flowing around it is equated to the force generated at the wire cross section to balance it.

$$\int_0^{\Delta L} \underbrace{\frac{\sigma_{weld}}{2}}_{\substack{\text{estimated}\\ \text{shear}\\ \text{stress}}} \underbrace{(2\pi r dx)}_{\substack{\text{area}\\ \text{increment}}} \sim \underbrace{\sigma_{wire}}_{\substack{\text{wire}\\ \text{stress}}} \underbrace{(\pi r^2)}_{\substack{\text{cross-section}\\ \text{area}}} \qquad \textbf{(2a)}$$

$$\pi \sigma_{weld} r \Delta L \sim \pi \sigma_{wire} r^2 \qquad \textbf{(2b)}$$

$$\Delta L \sim r \frac{\sigma_{wire}}{\sigma_{weld}} \qquad \textbf{(2c)}$$

Again if σ_{wire} is taken as the fracture stress of the wire, ΔL is the length at which the wire fractures and the length of the broken wire segments trailing the pin-tool.
Peak temperatures of 450°C, about 85% of the melting temperature, have been reported [8] in a 6061 aluminum FSW. Presumably this is close to the temperature of the shear zone where plastic work generates the heat. Temperatures generated in the FSW of 2195 aluminum alloy used in the present experiment are expected to be similar in magnitude. This is on the order of 20% of the melting temperature of tungsten, which should be unaffected at these temperatures. Given a reported [9] shear strength of drawn tungsten wire at 58 ksi, we can estimate σ_{wire} at 116 ksi. The strength of the 2195 weld metal will be substantially below its room temperature values at the shear zone temperatures. Assuming that the weld stress, σ_{weld}, is on the order of 5 ksi, then a flexible 0.0025 inch diameter (r = 0.00125 inches) wire breaks into 0.03 inch pieces according to equation 2. A stiff wire of the same size breaks into 0.002 inch pieces.

Experimental Procedure.

A 0.0025-inch diameter tungsten wire marker was placed along a weld seam at the mid-plane position of a pair of plates of 2195 aluminum-lithium alloy. Dimensions of the rolled plate were 6-inches wide, 24-inches long, and 0.33-inches thick. The seam was along the rolling direction of the plates. The plates were pressed together clamping the wire and GTA tack-welded to hold the plates in place. The plates were then clamped to the anvil bed of a FSW apparatus and an initial partial-penetration surface FSW, 0.05-inches deep, was made along the surface of the weld seam. The partially joined plates were then removed and wire placement was visually verified at the plate edges.

The plates were then attached to the anvil bed of the FSW apparatus and a full penetration weld was made along the seam with a weld tool 0.32-inches long. Figures 6 and 7 are lateral and plan views respectively of x-ray radiographs showing the condition of the wire after welding.

Wire segment dimensions and spacing were verified by serial sectioning metallographic studies. using Keller's regent to reveal the microstructural.

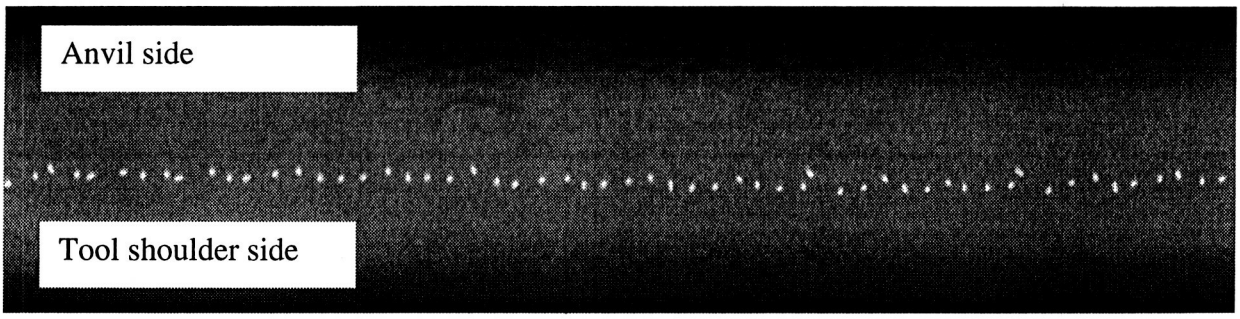

Figure **6**: Lateral-view radiograph of tungsten wire subjected to FSW.

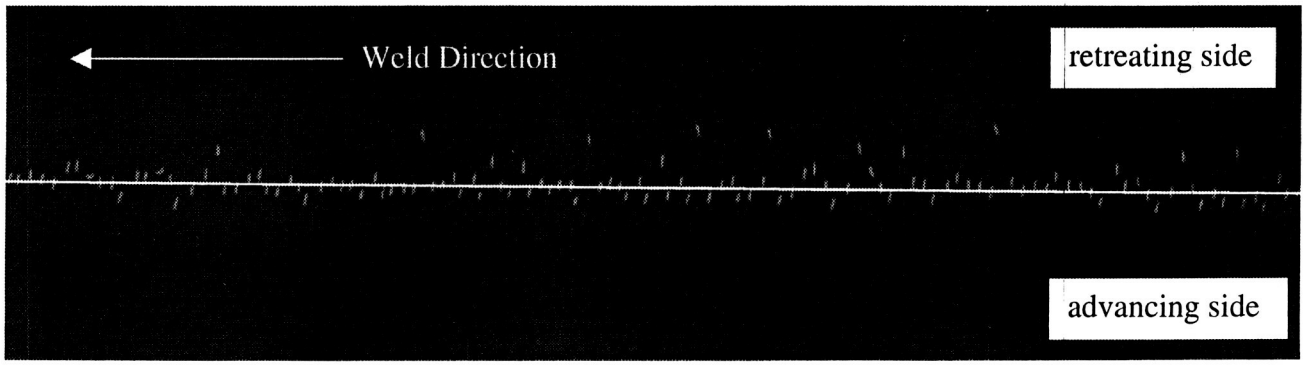

Figure **7**: Plan-view radiograph of tungsten wire subjected to FSW with white line showing the location of the initial weld seam. Wire segments are a uniform 0.026-inches in length, and spaced 0.020 to 0.028-inches apart.

Results and Discussion

The FSW tool breaks the wire into uniform segments, 0.026-inch in length. This is closer to the result of equation 2 than equation 1. This suggests a flexible wire broken in tension by a weld metal flow stress on the order of 11.6 ksi.

The wire break up during FSW and the pattern traced out is similar to results shown by Colligan using 0.015-inch diameter shot. The breakup of the wire, provides some

additional information on weld metal flow stress at the shear zone. Figure 8 shows a transverse section of the broken wire showing slight necking at the edges. A slight necking at the edges is indicative of a tensile failure mode.

The wire segments lie principally in the plan section and are oriented at an angle approximately perpendicular to the weld seam. Measurements obtained from serial sectioning of the FSW, show the spacing between segments ranges from 0.020 to 0.028-inches, approximately the length of the broken segments. This suggests that the weld metal flow close to the tool rotates the wire segments along the rotational flow direction and then abandons the segments behind the tool with the same orientation. It is consonant with a flexible wire model. The weld direction is from right to left in Figure 6, with the tool rotating clockwise. The outlying segment angles fall on a circular envelope of the same diameter as the tool.

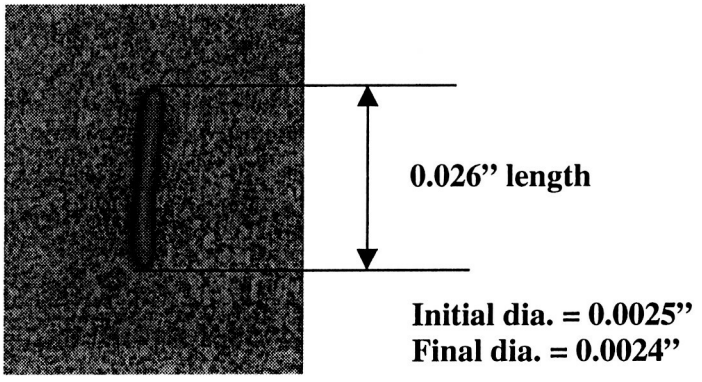

Figure 8. Section of embedded tungsten wire segment broken during the FSW process.

Most of the wire segments in the wake of the weld are arrayed in a straight line continuing the streamline along which the wire approaches the tool. A rigid body rotation at the tool superposed upon a uniform translation would exhibit the same flow pattern of streamlines in the plan view. The wire was placed near the center of the plate, where the ring vortex circulation has a negligible inward or outward component. At this level a mainly downward component of the ring vortex circulation would be expected. With a downward component only the streamline in the wake would be lowered by a maximum of half a thread pitch with respect to the approaching streamline.

The irregularities and occasional out-lying wire segments along the wake streamline may be due to small variations in the initial position of the wire. A small excursion into a region of inward or outward radial flow component of the ring vortex flow could result in a substantial displacement away from the streamline in the plan-view. The most distant outliers were displaced towards the advancing edge of the tool at a distance of a half pin radius or less from the weld centerline.

The rolled 2195 aluminum metal surrounding the wire segments was also affected by the thermo-mechanical process that broke the wire into pieces. The 60 to 80 micron diameter grains seen in plan-view were refined to approximately 10-micron diameter equiaxed grains.

Conclusions

A fine tungsten wire can serve as a marker to trace the flow patterns in friction stir welds in aluminum alloys in the same way that shot tracers have been used in the past with the following advantages:

- Better flow resolution if the wire diameter can be made appreciably smaller than the shot diameter.
- Information on the flow stress of the weld metal close to the FSW tool from the wire fragment size.
- More convenient handling.

The observed flow pattern is consistent with the macroscopic model of FSW flow synthesized at MSFC.

The 60 to 80 micron diameter pancake grains in a rolled 2195 aluminum alloy plate were refined to approximately 10-micron diameter equiaxed grains.

References

1 W.M. Thomas et al., "Friction Stir Butt Welding," (1991) U.S. Patent No. 5,460,317.

2 A.C. Nunes, Jr., "Wiping Metal Transfer in Friction Stir Welding", *Aluminum 2001: Proceedings of the 2001 TMS Annual Meeting Automotive Alloys and Joining Aluminum Symposia.* (New Orleans, LA, February 11-15). Edited by G. Kaufmann, J Green, and S. Das. TMS (The Minerals, Metals & Materials Society). (2001), 235-248.

3 K.N. Krishnan, "On the formation of onion rings in friction stir welds," Mat. Sci. & Engr. A, 327A (2002), 246-251.

4 Y. Li, L.E. Murr, J.C. McClure, "Solid State Flow Visualization in the Friction Stir Welding of 2024 Al to 661 Al," Scripta Mater., 40 (9) (1999), 1041-1046.

5 Y. Li, L.E. Murr, J.C. McClure, "Flow Visualization and Residual Microstructures Associated with the Friction-Stir Welding of 2024 Aluminum to 6061 Aluminum," Mat. Sci. & Engr. A, 271A (1999), 213-223.

6 K. Colligan, "Material Flow Behavior during Friction Stir Welding of Aluminum," Welding Research (1999), 229s-237s.

7 T.U. Seidel, A.P. Reynolds, "Visualization of the Material Flow in AA 2195 Friction-Stir Welds using a Marker Insert Technique," Met. & Mat. Trans. A, 32A (2001), 2879-2884.

8 W. Tang et al., "Heat Input and Temperature Distribution in Friction Stir Welding," J. Mat. Proc. & Mfgt. Sci., (1998) 163-172.

9 Materials Information Website, http:\\www.matweb.com.